

THE RESULTS OF OSCILLATION ANALYSIS IN K2K EXPERIMENT AND AN OVERVIEW OF JHF- ν EXPERIMENT

Issei Kato

for the K2K collaboration

Department of Physics, Faculty of Science, Kyoto University, Sakyo-ku, Kyoto 606-8502, Japan



This paper presents the results of oscillation analysis in K2K experiment. The results show indications of neutrino oscillation and give a new constraint on the oscillation parameters. The difference of neutrino masses squared Δm^2 lies between 1.5 and 3.9×10^{-3} eV 2 at $\sin^2 2\theta = 1$ with the confidence level of 90%. In addition to these results, a brief overview of future long-baseline neutrino experiment in Japan, JHF- ν experiment, is also given in this paper.

1 Introduction

Since a discovery of neutrino oscillation in atmospheric neutrinos by Super-Kamiokande (SK)¹, a lot of attention has been directed to this new phenomena. The zenith angle distribution of atmospheric neutrinos observed in SK shows a clear deficit of upward-going ν_μ , which is well explained by two-flavor ν_μ - ν_τ oscillation with $\Delta m^2 \sim 3 \times 10^{-3}$ eV 2 and $\sin^2 2\theta \sim 1$.

The KEK-to-Kamioka long-baseline neutrino experiment (K2K) uses an accelerator-produced neutrinos with a neutrino flight length of 250 km to probe the same Δm^2 region as that explored by atmospheric neutrinos. Recently, we have performed analysis for neutrino oscillation using the information of ν_μ flux at SK together with the shape of energy spectrum. This analysis is based on the data taken from June, 1999 to July 2001 (K2K-I) corresponding to 4.8×10^{19} protons on target (POT), which is approximately half of allocated POT. Since there already exist a lot of descriptions on K2K experiment^{2,3,4,5}, only the procedure of oscillation analysis and its results are presented in this paper. The description in this paper is based on the publication⁶.

While the first generation neutrino oscillation experiments have successfully been done and the oscillations in the atmospheric and solar region are confirmed by several experiments, ν_μ - ν_e oscillation has not been seen except for LSND and is still in mystery. In order to discover the ν_μ -

ν_e oscillation and to open possibilities for detailed studies of neutrino mass, lepton sector mixing and farther possibilities for discovery of new physics, JHF-to-Kamioka long-baseline neutrino experiment, JHF- ν , is planned in Japan as a next generation neutrino experiment. A brief overview of JHF- ν experiment is given in the last section.

2 Strategy for Oscillation Analysis in K2K

The neutrino beam in K2K experiment is produced by a 12 GeV proton beam from the KEK proton synchrotron. After protons hit an aluminum target, the produced positively charged particle, mainly π^+ , are focused by a pair of pulsed magnetic horns⁷. The pion momentum and angular distributions downstream of second horn are occasionally measured by gas-Cherenkov detector (PIMON)⁸ in order to verify the beam Monte Carlo (MC) simulation and to estimate the errors on the flux prediction at SK². The neutrino beam produced from the decays of these particles in a decay pipe of 200 m long are 98% pure muon neutrinos with a mean energy of 1.3 GeV. Near neutrino detectors (ND) are located at 300 m from the proton target. ND measure the stability and direction of the neutrino beam as well as neutrino flux and energy spectrum just after the production. SK is located at 250 km from KEK. Here the neutrino flux and energy spectrum after neutrinos travel the length of 250 km are measured. The measurements at ND are extrapolated to SK by multiplying far-to-near flux ratio (F/N). The detailed description for F/N can be found in the reference².

In the case of the presence of neutrino oscillation, both the reduction in the number of neutrino events and the distortion in the energy spectrum are expected after neutrinos travel a fixed flight length, because the oscillation probability depends on neutrino energy:

$$P(\nu_\mu \rightarrow \nu_x) = \sin^2 2\theta \sin^2 \frac{\Delta m^2 L}{4E_\nu}, \quad (1)$$

where θ is mixing angle, Δm^2 is the difference of neutrino mass squared, E_ν is neutrino energy, and L is the neutrino flight length which is fixed to be 250 km in the K2K case. Therefore both the number of observed events and the spectral shape information at SK are used to compare them with the expectation from ND measurements. In this analysis, all the beam induced neutrino events observed in the fiducial volume of SK are used to measure the overall suppression of flux, while in order to enhance the fraction of charged-current (CC) quasi-elastic (QE) interactions ($\nu_\mu + n \rightarrow \mu + p$), 1-ring μ -like events (1R μ) are used to study the spectral distortion. Since the proton momentum in the CCQE events is typically below Cherenkov threshold, only muon is visible. Assuming QE interaction in 1R μ and neglecting Fermi momentum, the neutrino energy can be reconstructed as

$$E_\nu^{\text{rec}} = \frac{m_N E_\mu + m_\mu^2}{m_N - E_\mu + p_\mu \cos \theta_\mu}, \quad (2)$$

where m_N , E_μ , m_μ , p_μ and θ_μ are nucleon mass, muon energy, muon mass, muon momentum and muon scattering angle with respect to the direction of neutrino beam, respectively.

3 Measurements of Neutrino Flux and Spectrum at ND

The ND consist of two detector systems: a 1 kilo-ton water Cherenkov detector (1KT) and a fine-grained detector (FGD). The flux normalization is measured by 1KT to estimate the expected number of events at SK. Since 1KT has the same detector technology as SK, the most of the systematic uncertainties on the measurements, mainly on the detection efficiency and cross-section of interactions, are canceled in comparison between ND and SK measurements.

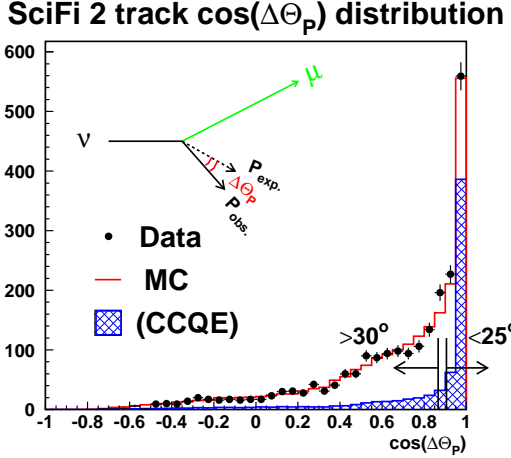


Figure 1: The distribution of $\cos \Delta\theta_p$ for 2-track sample in SciFi. The schematic explanation for $\Delta\theta_p$ is also drawn. The events with $\Delta\theta_p < 25$ deg. are selected as QE enhanced sample, while those with $\Delta\theta_p > 30$ deg. are selected as non-QE enhanced sample.

The energy spectrum is measured by analyzing the muon momentum and angular distributions in the both detector systems. The 1KT has high efficiency to reconstruct muons with the momentum of below 1 GeV/c and full 4π coverage in solid angle. However, the 1KT has little efficiency to reconstruct muons with the momentum of above 1.5 GeV/c since they exit the detector. On the other hand, the FGD has high efficiency to measure the muons above 1 GeV/c, the relevant energy range can be covered by these two complementary detectors.

3.1 1KT Analysis

In the 1KT analysis, the ν_μ interactions are measured by detecting Cherenkov light emitted from produced charged particles. The vertices, direction and momentum of Cherenkov rings are reconstructed with the same method as in SK⁹. The event selection criteria for the measurement of integrated flux are the same as those in the reference²: (a) Deposited energy is greater than 100 MeV. (b) The reconstructed vertex is inside the 25 t fiducial volume which is defined by a 2 m radius, 2 m long cylinder oriented to the beam axis, in the upstream side of the detector. The expected number of events with the vertices fully contained (FC) in SK fiducial volume is estimated to be $80.1^{+6.2}_{-5.4}$. The correlation between energy bins from the spectrum measurement at ND and F/N are taken into account in the estimation of the errors, described in detail below. The major contribution to the errors come from the uncertainties in the F/N ($^{+4.9\%}_{-5.0\%}$) and the normalization ($\pm 5\%$). The normalization error is dominated by uncertainties of the fiducial volumes due to the vertex reconstruction both in 1KT (4%) and in SK (3%). For the spectrum measurement, we impose further cuts in order to select 1R μ events: (c) The event has one ring. (d) The particle stops inside the 1KT. Among the events after the cuts (a) and (b), 53% have one ring. For criteria (d), we require the maximum charge of hit photomultiplier tubes (PMT) to be less than 200 p.e. This eliminates effectively the events with muon exiting the 1KT; 68% of one ring events retain after this cut. Using this sample, we make the muon momentum and angular distributions to estimate the spectrum shape of neutrino, which is described in detail below. The largest systematic uncertainty for the spectrum measurement in the 1KT is that on energy scale. We estimate the error on energy scale using cosmic-ray muons and beam-induced π^0 sample and quote $^{+2\%}_{-3\%}$ for this error.

Table 1: The central values of the flux re-weighting parameters for the spectrum fit at ND (Φ_{ND}) and the percentage size of the energy dependent systematic errors on Φ_{ND} , F/N , and ϵ_{SK} . The re weighting parameters are given relative to the 1.0–1.5 GeV energy bin.

E_{ν} (GeV)	Φ_{ND}	$\Delta\Phi_{\text{ND}}$	$\Delta(F/N)$	$\Delta\epsilon_{\text{SK}}$
0–0.5	1.31	49	2.6	8.7
0.5–0.75	1.02	12	4.3	4.3
0.75–1.0	1.01	9.1	4.3	4.3
1.0–1.5	≡ 1.00	—	6.5	8.9
1.5–2.0	0.95	7.1	10	10
2.0–2.5	0.96	8.4	11	9.8
2.5–3.0	1.18	19	12	9.9
3.0–	1.07	20	12	9.9

3.2 FGD Analysis

The FGD consist of a scintillating fiber tracker with water target (SciFi)³, plastic scintillator trigger counters upstream and downstream of SciFi (TRIG), a lead-glass calorimeter (LG), and a muon range detector (MRD)⁴. In the FGD analysis, we use the events which have one or two tracks with the vertex within the 5.9 t fiducial volume of SciFi, which is defined as a rectangle of 2.2 m × 2.2 m in x and y , and 1st to 17th water containers in the beam direction (z). The track finding efficiency is 70% for a track passing through three layers of SciFi and close to 100% for more than five layers¹⁰. Three layers is the minimum track length required in this analysis. Events which have at least one track passing into MRD are chosen in order to select ν_{μ} -induced CC interactions. Furthermore since SciFi and MRD do not have fine timing information to select on-spill events, it is required that the hit in downstream TRIG which matches with SciFi track should be in spill timing. The momentum of each track is measured by its range through the SciFi, TRIG, LG and MRD with the accuracy of 2.7%. The second track also be reconstructed if the proton produced in the QE interaction has a momentum of typically greater than 600 MeV/ c . In the case where the second track is visible, the kinematical information is used to enhance the fraction of QE and non-QE events in the sample. The direction of second track can be predicted from the momentum of the first track by assuming QE interaction. The distribution of cosine of the angular difference between the predicted and observed second track ($\cos \Delta\theta_p$) is shown in Fig. 1. QE enhanced and non-QE enhanced samples are selected by requiring $\Delta\theta_p < 25$ deg. and $\Delta\theta_p > 30$ deg., respectively. The fraction of the QE events in the QE sample is estimated to be 62% by MC simulation, while 82% of events in non-QE sample is estimated to come from interactions other than QE. The SciFi events are divided into three event categories; 1-track, 2-track QE enhanced, and 2-track non-QE enhanced samples. We make muon momentum and angular distributions for each event category to estimate the neutrino energy spectrum at ND, which is described below.

3.3 Neutrino Spectrum at ND

In order to estimate the neutrino energy spectrum at ND, i.e. just after the production, the 2-dimensional distributions of muon momentum and angle with the respect to the neutrino beam direction for four event categories are used: 1R μ sample in 1KT, 1-track, 2-track QE enhanced, and 2-track non-QE enhanced samples in FGD. A χ^2 -fitting method is used to compare these data against the MC expectation. The neutrino spectrum is divided into eight energy bins as defined in Table 1. The flux in each energy bin is re-weighted relative to the value of the beam MC simulation. These re-weighting parameters are normalized such as the bin of $E_{\nu} = 1.0$ –

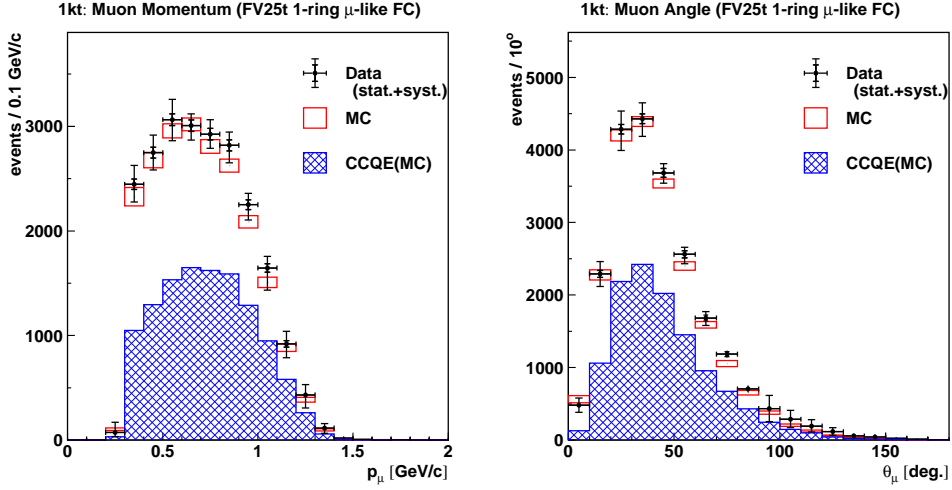


Figure 2: The momentum and angular distributions for 1KT 1R μ sample. The left figure is the distribution of momentum and the right one is that of angle with respect to the beam direction. The hatched histograms are the contribution from CCQE interaction in MC simulation.

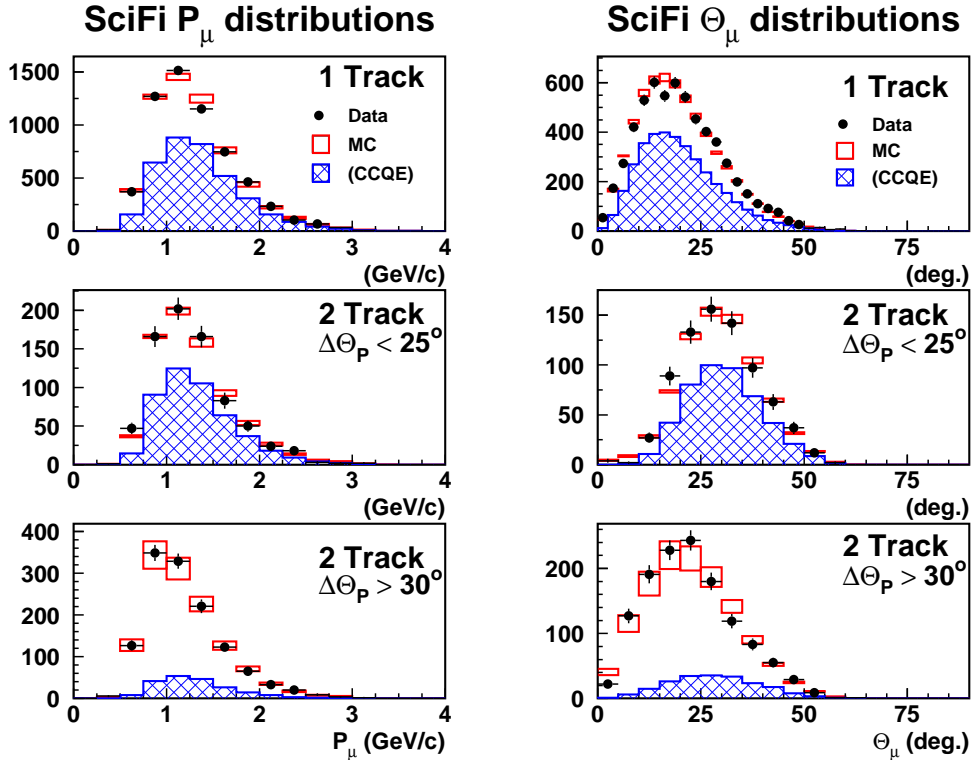


Figure 3: The momentum and angular distributions for SciFi event samples. The left figures are the distributions of momentum and the right ones are those of angle with respect to the beam direction for 1-track, 2-track QE enhanced, and 2-track non-QE enhanced samples in order of the top, middle, and bottom figures. Here again, the hatched histograms are contribution from CCQE interaction in MC simulation.

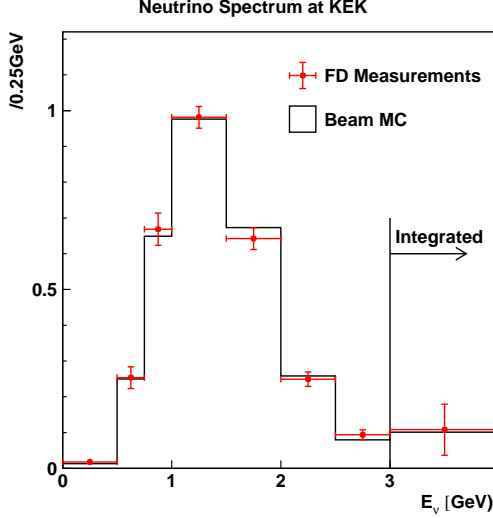


Figure 4: The neutrino energy spectrum at near site inferred from ND data along with the result of beam MC simulation. Points with error bars are the resulting spectrum of ND fitting, while histogram is the result of beam MC simulation.

1.5 GeV to be 1.0. An overall normalization is introduced as a free parameter in the fit. The parameter R_{nqe} is used to re-weight the ratio between the QE and non-QE cross-section relative to the MC simulation. The systematic uncertainties in the ND measurements, such as the energy scales, the track finding efficiencies, the detector thresholds, and so on, are incorporated into the fitting. In addition, PIMON is used in order to constrain the re-weighting parameters for $E_\nu > 1.0$ GeV.

The fitting is successfully done, and the χ^2 value at the best-fit point is 227.2/197d.o.f. All the parameters including the detector systematics are found to lie within their expected errors. The best-fit values of the flux re-weighting factors are shown in Table 1. The muon momentum and angular distributions for $1R\mu$ sample in 1KT and for 1-track, 2-track QE enhanced and 2-track non-QE enhanced samples are shown in Fig. 2 and 3 with the re-weighted MC overlaid. The fitting results are in good agreement with the data. The resulting neutrino spectrum inferred from the ND data is shown in Fig. 4 along with the beam MC simulation result. As can be seen, the results of beam MC excellently agrees with ND measurements. The errors on this measurement are provided in the form of an error matrix, and the correlations between the parameters are taken into account in the oscillation matrix using this matrix, later described in detail. The diagonal elements of the error matrix are shown in Table 1.

3.4 Neutrino Interaction Models

The uncertainty due to neutrino interaction models is studied separately. In QE interaction, the axial vector mass in the dipole formula is set to be $1.1 \text{ GeV}/c^2$ as a central value and is varied by $\pm 10\%$. In single pion production, the central value of the axial vector mass is set to be $1.2 \text{ GeV}/c^2$ and varied by $\pm 20\%$ ¹¹. For coherent pion production, two different models are compared: One is the Rein and Sehgal model¹² and the other is a model by Marteau *et al.*¹³. For deep inelastic scattering, GRV94¹⁴ and the corrected structure function modeled by Bodek and Yang¹⁵ are studied. Marteau model for coherent pion production and Bodek and Yang structure function for deep inelastic scattering are employed in this analysis. The choice of models causes the fitted value of R_{nqe} to change by $\sim 20\%$. Therefore, the error of 20% on R_{nqe} is added to the error matrix. It is found that the choice of models and axial vector mass does not affect on the result of spectrum measurement beyond the size of the fitted errors.

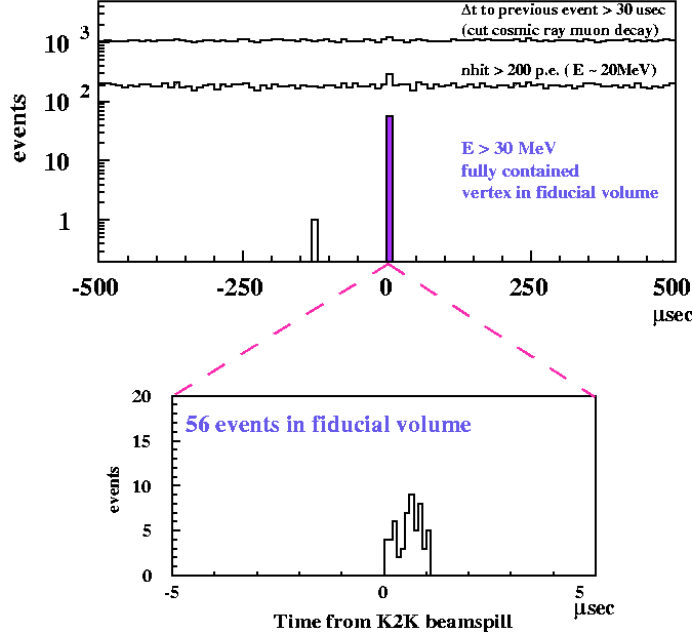


Figure 5: The distribution of $\Delta T (\equiv T_{\text{SK}} - T_{\text{KEK}} - T_{\text{TOF}})$ for FC events in SK. The upper figure shows the distribution of $\pm 500 \mu\text{sec}$ time window for each reduction step in SK. The lower figure shows the distribution of $\pm 5 \mu\text{sec}$ time window for FCFV events.

4 Far-to-near Spectrum Ratio

The F/N ratio from the beam MC simulation is used to extrapolate the measurement at ND to those at SK. The detailed description about F/N can be found in the reference². The errors on F/N are also provided in the form of an error matrix. The errors including the correlations on F/N for $E_\nu > 1 \text{ GeV}$ are estimated based on the PIMON measurements, where PIMON is sensitive in this energy region. Since PIMON is insensitive in the region of $E_\nu < 1 \text{ GeV}$, the errors and correlations are estimated based on the uncertainties in the hadron production models used in K2K beam MC simulation. The errors on F/N of $E_\nu > 1 \text{ GeV}$ and on that of $E_\nu < 1 \text{ GeV}$ are treated such that these are not correlated. The diagonal elements in the error matrix are summarized in Table 1.

5 Event Selection in SK

The selection criteria for SK events are all same as those described in the reference². Accelerator-produced neutrino interaction at SK are selected by comparing two Universal Time Coordinated (UTC) time stamps from the global positioning system (GPS), T_{KEK} for the KEK-PS beam spill start time and T_{SK} for the SK trigger time. The time difference between two UTC time stamps, $\Delta T \equiv T_{\text{SK}} - T_{\text{KEK}} - T_{\text{TOF}}$, where T_{TOF} is the time of flight of neutrinos from KEK to SK, should be distributed around the interval from 0 to $1.1 \mu\text{sec}$ to match the width of the beam spill of KEK-PS. The condition $-0.2 < \Delta T < 1.3 \mu\text{sec}$ is imposed as a timing cut. Other criteria are: (a) There is no detector activity within $30 \mu\text{sec}$ before the event. (b) The total collected p.e. in a 300 nsec time window is greater than 200 ($\sim 20 \text{ MeV}$ deposited energy). (c) The number of PMTs in the largest hit cluster in the outer-detector is less than 10. (d) The deposited energy is greater than 30 MeV . Finally, a fiducial cut is applied to select only the events with fitted vertices inside 22.5 kt fiducial volume, which volume is same as that used in SK atmospheric neutrino analysis. The detection efficiency of this selection is 93% for charged-

current interactions and 68% for neutral-current inelastic interactions, for a total of 79%. Fig. 5 shows the ΔT distribution at the various stages of the reduction. A clear peak in time with the neutrino beam from KEK-PS is observed in the analysis time window. After the above selection, 56 FC events are observed in the fiducial volume (FCFV events), while the number of FCFV events expected by 1KT measurement is $80.1^{+6.2}_{-5.4}$ as described in Sec. 3.1. With the timing cut, the expected number of atmospheric neutrino background is approximately 10^{-3} event, which is negligible.

6 Oscillation Analysis

A two-flavor oscillation analysis, with ν_μ disappearance, is performed with the use of the maximum-likelihood method. In this analysis, both the number of FCFV events and the energy spectrum shape for 1R μ are used. The likelihood is defined as

$$\mathcal{L}_{\text{tot}} = \mathcal{L}_{\text{norm}}(N_{\text{obs}}, N_{\text{exp}}(\Delta m^2, \sin^2 2\theta, f)) \times \mathcal{L}_{\text{shape}}(\Delta m^2, \sin^2 2\theta, f) \times \mathcal{L}_{\text{sys}}(f). \quad (3)$$

The normalization term $\mathcal{L}_{\text{norm}}$ is the Poisson probability to observe N_{obs} events when the expected number of events is $N_{\text{exp}}(\Delta m^2, \sin^2 2\theta, f)$. The spectrum shape term $\mathcal{L}_{\text{shape}}$ is the product of the probability for each 1R μ event to be observed at $E_\nu^{\text{rec}} = E_i$:

$$\mathcal{L}_{\text{shape}} = \prod_{i=1}^{N_{1R\mu}} P(E_i; \Delta m^2, \sin^2 2\theta, f), \quad (4)$$

where P is the normalized *Enurec* distribution estimated by MC simulation and $N_{1R\mu}$ is the number of 1R μ events. The symbol f denotes a set of parameters which is constrained by the systematic errors. These parameters consist of the re-weighted neutrino spectrum measured by ND (Φ_{ND}), the F/N ratio, the reconstruction efficiency of SK (ϵ_{SK}) for 1R μ events, the re-weighting factor for the QE/non-QE ratio R_{nqe} , the energy scale of SK, and the overall normalization. The errors on first three items are energy dependent and correlated between each energy bin. The diagonal elements of their error matrices are summarized in Table 1. The error on SK energy scale is 3%. The parameters f is treated as fitting parameters with an additional constraint term \mathcal{L}_{sys} in likelihood^a.

In the oscillation analysis, the whole data sample is used in the normalization term $\mathcal{L}_{\text{norm}}$, i.e. $N_{\text{obs}} = 56$. In the spectrum shape term $\mathcal{L}_{\text{shape}}$, the data taken in June 1999 are discarded since the target radius and horn current, hence the spectrum shape in June 1999 were different from the rest of running period. The discarded data correspond to 6.5% of total POT. The number of 1R μ events used in this analysis is 29, while the number of 1R μ events from the MC simulation in the case of no oscillation is 44.

The likelihood is calculated at each point in the Δm^2 and $\sin^2 2\theta$ space to search for the point where the likelihood is maximized. The best-fit point in the physical region of oscillation parameter space is found to be at $(\sin^2 2\theta, \Delta m^2) = (1.0, 2.8 \times 10^{-3} \text{ eV}^2)$. If the whole space including unphysical region is allowed, these values are found to be $(\sin^2 2\theta, \Delta m^2) = (1.03, 2.8 \times 10^{-3} \text{ eV}^2)$. At the best-fit point in the physical region, the total number of predicted events is 54.2, which is in agreement with the observation of 56 events within statistical error. The observed E_ν^{rec} distribution for 1R μ sample is shown in Fig. 6 together with the expectation for the best-fit oscillation parameters and that for no oscillation. The Kolgomorov-Smirnov (KS) test is done to check the consistency between the observed and best-fit E_ν^{rec} spectrum. A KS probability is obtained to be 79%, and the best-fit spectrum shape agrees with the observation.

^aAnother approach to treat the systematic parameters f is performed, which also gives consistent results with those described in the main text⁶.

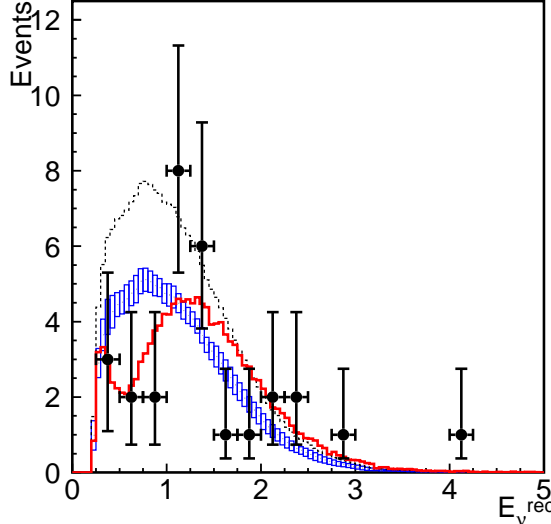


Figure 6: The reconstructed E_ν distribution for the 1R μ sample (from method 1). Points with error bars are data, while the box histogram is the expected spectrum in the case of no oscillation, where the height of the box is the systematic error. The solid line is the best-fit spectrum in the case where the oscillation occurred. These histograms are normalized by the number of observed 1R μ events (29). In addition, the dashed line shows the expectation with no oscillation normalized to the expected number of 1R μ events (44).

The likelihood ratio of the no oscillation case to the best-fit point is computed to estimate the probability that the observations are only due to a statistical fluctuation instead of neutrino oscillation. The no oscillation probability is calculated to be 0.7%. When only normalization or shape information is used, the probabilities are 1.3% and 16%, respectively. The oscillation parameters preferred by the total flux suppression and the energy distortion alone also agree well with each other (Fig. 7 (right)). The allowed regions of oscillation parameters are evaluated by calculating the likelihood ratio of each point to the best-fit point.

Finally the uncertainties of neutrino interaction models are studied in the same way as the spectrum measurement at ND. It is found that the effects of difference between interaction models are negligible for all the results since the cancellation is caused by using the same models in ND and SK.

The contours for confidence level of 68%, 90%, and 99% are drawn in Fig. 7 (left). The behaviors of $-\Delta(\ln \mathcal{L}_{\text{tot}})$ in the case where normalization-only, shape-only, and normalization+shape information is used in the analysis are plotted in Fig. 7 (right). This shows that the reduction in the neutrino flux and the distortion in energy spectrum observed in K2K experiment prefer the same Δm^2 region with each other, as described above. $-\Delta(\ln \mathcal{L}_{\text{tot}})$ as a function of $\sin^2 2\theta$ at the best-fit Δm^2 ($= 2.8 \times 10^{-3}$ eV 2) and as a function of Δm^2 at the best-fit $\sin^2 2\theta$ ($= 1.0$) are also shown in Fig. 8. The 90% C.L. region of Δm^2 is $1.5\text{--}3.9 \times 10^{-3}$ eV 2 at $\sin^2 2\theta = 1.0$. The allowed region of oscillation parameters obtained by Super-Kamiokande atmospheric neutrino observations are also drawn in Fig. 7. The K2K and Super-Kamiokande results are in good agreement.

7 The Upgrade of K2K Near Detector — SciBar Detector —

In the case where the oscillation parameter is $\Delta m^2 \sim 3 \times 10^{-3}$ eV 2 , the neutrino energy for oscillation maximum is ~ 0.6 GeV under the condition of fixed flight length of 250 km. Therefore, precise measurement of neutrino spectrum and the knowledge of neutrino interaction in low energy region are indispensable in order to maximize the K2K sensitivity. However, low energy particles of which momentum is below Cherenkov threshold are invisible in the 1KT, while SciFi

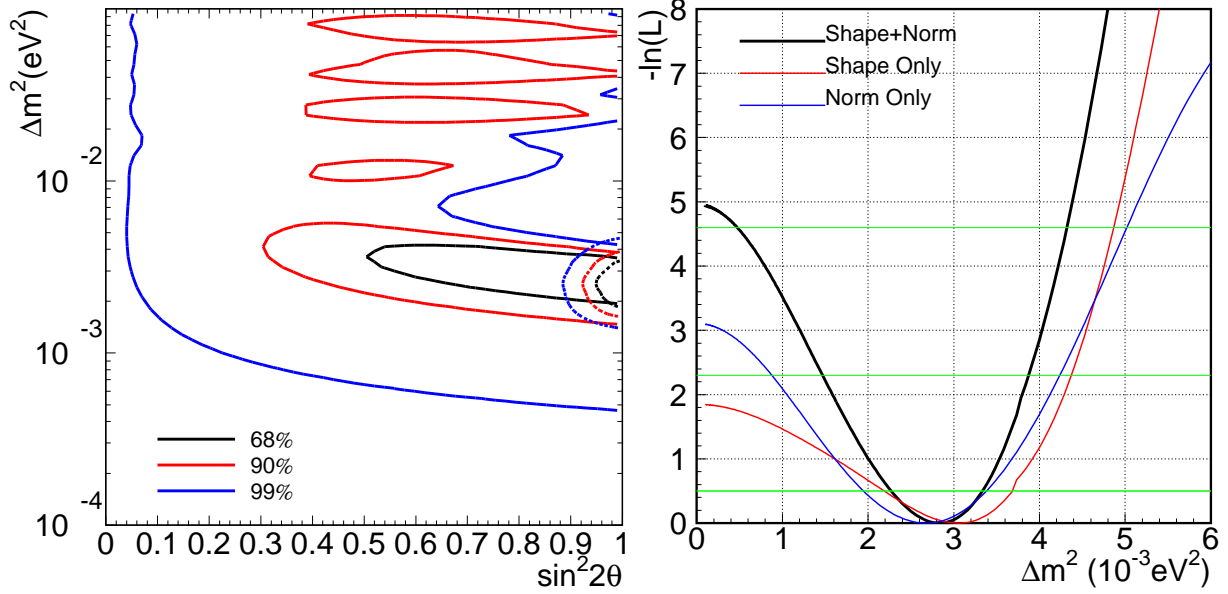


Figure 7: Left: Allowed region of oscillation parameters with the confidence level of 68%, 90%, and 99%. Solid lines are the results from the K2K oscillation analysis. In addition, the results of the observation of atmospheric neutrinos by Super-Kamiokande (dashed lines) are overlaid. Right: The Behaviors of $-\Delta(\ln \mathcal{L}_{\text{tot}})$ as a function of Δm^2 along $\sin^2 2\theta = 1.0$ axis in the case where normalization-only, shape-only, and normalization+shape information is used in the analysis. The Δm^2 regions indicated by normalization-only and shape-only agrees well with each other. region as analysis

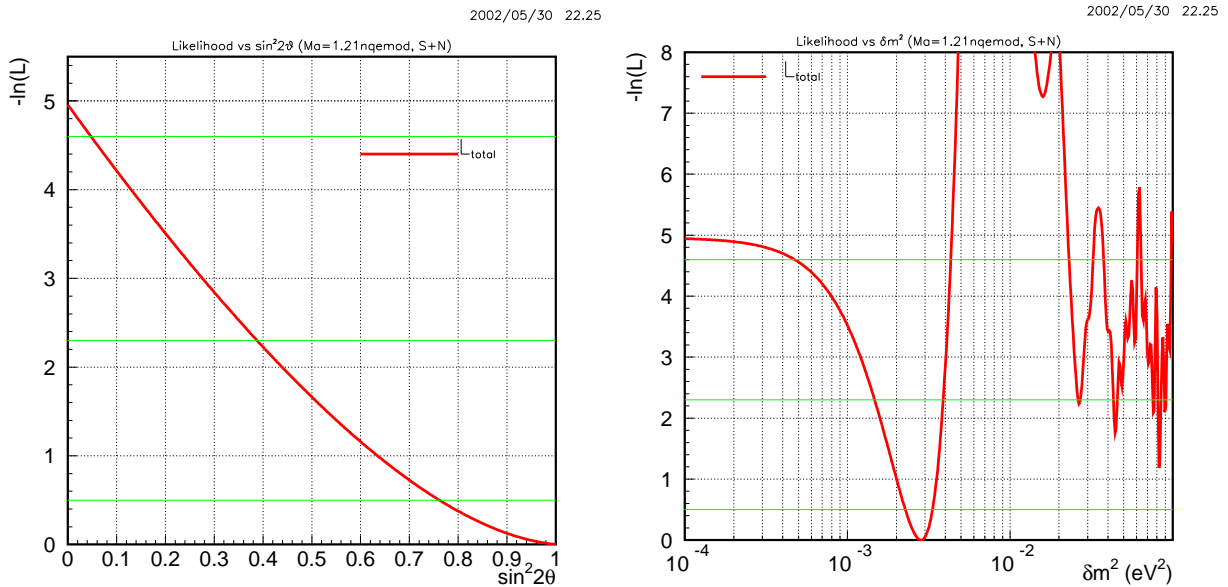


Figure 8: The behaviors of $-\Delta(\ln \mathcal{L}_{\text{tot}})$ as a function of $\sin^2 2\theta$ at $\Delta m^2 = 2.8 \times 10^{-3}$ eV 2 (left) and as a function of Δm^2 at $\sin^2 2\theta = 1.0$ (right).

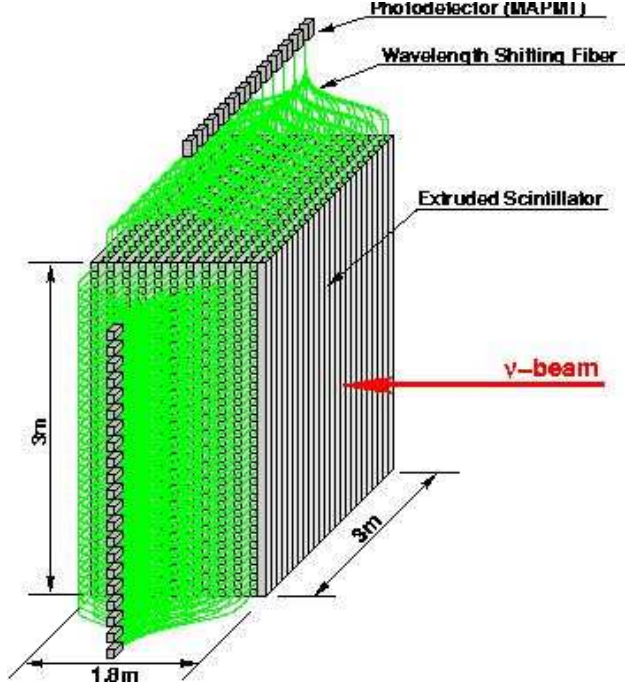


Figure 9: The schematic view of SciBar detector

have small efficiency for muons below 0.8 GeV/c.

As an upgrade of K2K near detector, SciBar detector is designed/developed to detect such low energy particles with high efficiency. The schematic view of SciBar detector is drawn in Fig. 9. The detector consists of extruded plastic scintillators which dimensions are 1.3 cm thick, 2.5 cm wide, and 3 m long. Scintillators are aligned in X or Y to construct a layer (X-layer or Y-layer). A pair of X- and Y-layer is called as a module, and 64 modules are aligned in z -direction, or beam direction. A hole of diameter of 1.8 mm is opened at the center of cross section along through each scintillator. A wavelength shifting fiber is put in this hole to readout the scintillation light from each scintillator. The light transmitted outside the scintillator is read by 64ch multi-anode photomultiplier tubes at one end of fibers.

The main feature of SciBar detector is that SciBar is a full-active tracker in which the scintillators play roles of both neutrino interaction target and particle detector at the same time. Therefore, SciBar has high efficiency for short tracks, can detect low energy protons down to 350 MeV/c. SciBar also measure dE/dx of each particle. Using this information, particle identifications and momentum reconstruction can be performed.

The following study can be done with the use of this excellent detector: Precise measurement of neutrino spectrum in low energy. Detailed study of neutrino interactions. Especially non-QE interactions are the background against neutrino energy reconstruction in CCQE, therefore to understand these background is very important to maximize the oscillation sensitivity.

Almost all the R&D items have been finished and the basic performances of the detector have been studied. Installation work will be done during the summer in 2003 and will be finished by the end of September 2003. The data taking will be started from the beam time of October 2003.

8 Overview of JHF- ν Experiment

The JHF to Kamioka neutrino project is a second generation long baseline neutrino oscillation experiment (JHF- ν experiment) that probes physics beyond the Standard Model by high preci-

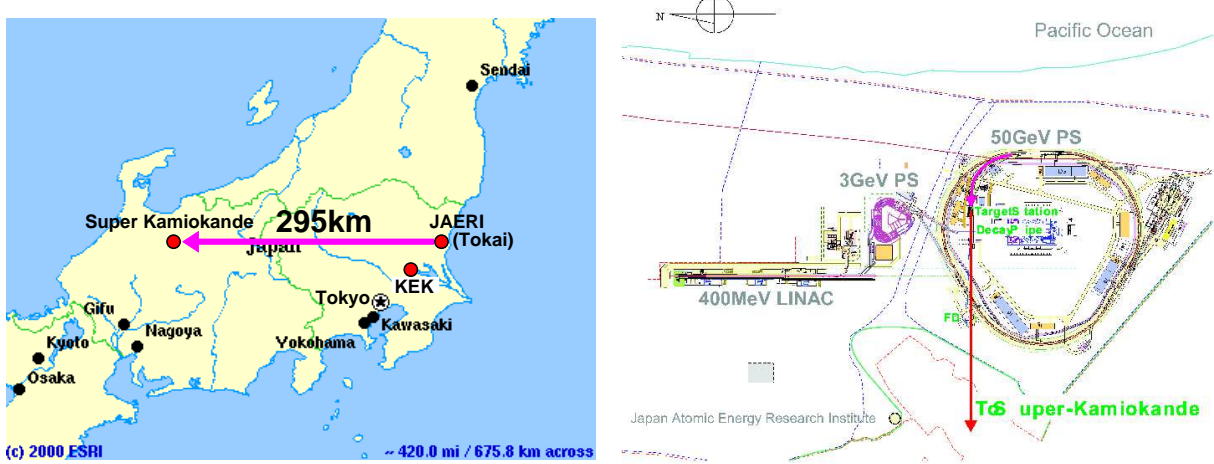


Figure 10: The baseline of JHF to Kamioka neutrino project (left) and the layout of JHF (right).

sion measurements of the neutrino masses and mixing. A high intensity narrow band neutrino beam is produced by secondary pions created by a high intensity proton synchrotron at J-PARC (JAERI). The neutrino energy is tuned to the oscillation maximum of ~ 1 GeV for a baseline length of 295 km toward the world largest water Cherenkov detector, Super-Kamiokande (left figure of Fig.10). Its excellent energy resolution and particle identification enable us to reconstruct the initial neutrino energy, which is compared with the narrow band neutrino energy, through the quasi-elastic interaction.

The JHF- ν experiment consists of two phases, phase-I and phase-II. The physics goal of the phase-I is a search for the $\nu_\mu \rightarrow \nu_e$ appearance with a factor of 20 higher sensitivity ($\sin^2 2\theta_{\mu e} \simeq 0.5 \sin^2 2\theta_{13} > 0.003$), the $\nu_\mu \rightarrow \nu_\tau$ oscillation measurement with an order of magnitude better precision ($\delta(\Delta m_{23}^2) = 10^{-4}$ eV 2 and $\delta(\sin^2 2\theta_{23}) = 0.01$) than existing measurements, and a confirmation of the $\nu_\mu \rightarrow \nu_\tau$ oscillation or discovery of sterile neutrinos (ν_s) by detecting the neutral current events. In the phase-II, an upgrade of the accelerator from 0.75 MW to 4 MW in beam power and the construction of 1 Mt Hyper-Kamiokande detector at Kamioka site are envisaged. By these upgrade, it is expected that improvement of another order of magnitude in the $\nu_\mu \rightarrow \nu_e$ oscillation sensitivity, a sensitive search for the CP violation in the lepton sector (CP phase δ down to 10° – 20°), and improvement of an order of magnitude in the sensitivity of the nucleon decay search.

The descriptions in this paper are all based on the “Letter of Intent for JHF Neutrino Experiment”¹⁶. Here only the items related to neutrino beam of JHF- ν experiment and the search for ν_e appearance. More detailed descriptions are found in the Letter of Intent.

8.1 Neutrino Beam at JHF

The layout of JHF is drawn in Fig. 10(right). The proton beam is fast-extracted from the 50 GeV PS in a single turn and transported to the production target. The design intensity of the PS is 3.3×10^{14} protons per pulse (ppp) at a repetition rate of 0.285 Hz (3.5 sec period). The resulting beam power is 0.75 MW (2.64 MJ/pulse). The spill width is ~ 5.2 μ sec. We define a typical one year operation as 10^{21} POT, which is corresponding to about 130 days of operation. The protons are extracted toward inside of the PS ring, and are bent by 90° to SK direction in the transport line using superconducting magnets. The secondary pions (and kaons) from the target are focused by electromagnetic horns¹⁷, and decay in the decay pipe. The length of the decay pipe from the target position is 130 m. The first near detectors are located at 280 m from

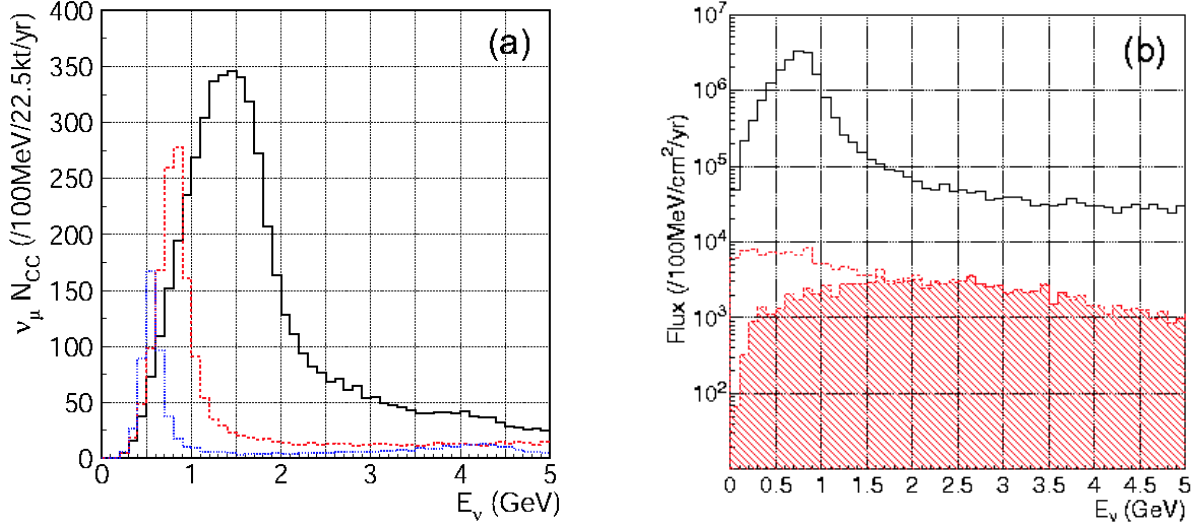


Figure 11: (a) Neutrino energy spectra of charged current interactions. Thick solid, dashed and dash-dotted histograms are OA1 $^\circ$, OA2 $^\circ$ and OA3 $^\circ$, respectively. (b) Comparison of ν_e and ν_μ spectra OA2 $^\circ$. Solid (black) histogram is ν_μ and dashed (red) one is ν_e . Hatched area is contribution from K decay. The low energy ν_e component is due to μ decay.

the target. There also exists a plan to put second near detectors (intermediate detectors) at 2 km from the target.

The beam configuration is off-axis beam (OAB) to produce a narrow neutrino energy spectrum¹⁸. The optics is almost same as the usual wide band beam, which is also used in K2K experiment, however, the axis of the beam optics is displaced by a few degrees from the direction of far detector (off-axis). A finite decay angle selected, the neutrino energy becomes almost independent of parent pion momentum as a consequence of the characteristics of the Lorenz boost, which provides the narrow spectrum. The peak energy of neutrino can be adjusted by choosing the off-axis angle. The distance between JHF and SK is 295 km. The neutrino energy will be tuned to between 0.4 and 1.0 GeV, which corresponds to Δm^2 between $1.6\text{--}4 \times 10^{-3}$ eV² suggested by recent SK and K2K results^{1,6}. Fig. 11(a) shows expected neutrino energy spectrum of charged current interactions at SK in MC simulation. The OAB is roughly a factor of 3 more intense than usual narrow band beam which is made by selecting the momentum of pions using dipole magnet placed between two horns. Fluxes and numbers of interactions are summarized in Table 2.

The ν_e contamination in the beam is expected to be 1% at the off-axis angle of 2 $^\circ$ (OA2 $^\circ$). The sources of ν_e are $\pi \rightarrow \mu \rightarrow e$ decay chain and K decay (K_{e3}). Their fractions are μ -decay: 37%, K-decay: 63% for OA2 $^\circ$. The energy spectra of the ν_e contamination are plotted in Fig. 11(b). At the peak energy of the ν_μ spectrum, the ν_e/ν_μ ratio is as small as 0.2% in OAB. This indicates that beam ν_e background is greatly suppressed (factor ~ 4) by applying an energy cut on the reconstructed neutrino energy.

8.2 Search for ν_e Appearance

The JHF neutrino beam has small ν_e contamination (0.2% at the peak energy of OAB) and the ν_e appearance signal is enhanced by tuning the neutrino energy to be its expected oscillation maximum. Therefore, JHF- ν experiment has an excellent opportunity to discover ν_e appearance and hence to measure θ_{13} . The sensitivity on ν_e appearance is studied based on the full MC simulations and analysis of SK and K2K experiments.

The ν_e appearance signal is searched for in the CCQE interaction, for which the energy

Table 2: Summary of ν_μ beam simulation. The peak energy E_{peak} is in GeV. The flux is given in $10^6/\text{cm}^2/\text{yr}$, and the ν_e/ν_μ flux ratio is in %. The ratio in the “total” column is the one integrated over neutrino energy and the column “ E_{peak} ” is the ratio at the peak energy of ν_μ spectrum. The normalization for the number of interactions are /22.5kt/yr. The numbers outside (inside) the bracket are number of total (CC) interactions.

Beam	E_{peak}	Flux		ν_e/ν_μ (%)		# of interactions	
		ν_μ	ν_e	total	E_{peak}	ν_μ	ν_e
OA2°	0.7	19.2	0.19	1.00	0.21	3100(2200)	60(45)
OA3°	0.55	10.6	0.13	1.21	0.20	1100(800)	29(22)

Table 3: Number of events and reduction efficiency of “standard” 1-ring e-like cut and π^0 cut for 5 year exposure (5×10^{21} POT) OA2°. For the calculation of oscillated ν_e , $\Delta m^2 = 3 \times 10^{-3}$ eV 2 and $\sin^2 2\theta_{\mu e} = 0.05$ is assumed.

OAB 2°	ν_μ CC	ν_μ NC	Beam	ν_e	Oscillated ν_e
(1) Generated in F.V.	10713.6	4080.3		292.1	301.6
(2) 1R e-like		14.3	247.1	68.4	203.7
(3) e/ π^0 separation		3.5	23.0	21.9	152.2
(4) $0.4 \text{ GeV} < E_\nu^{\text{rec}} < 1.2 \text{ GeV}$	1.8	9.3	11.1		123.2

of neutrino can be calculated using kinematics. Since the proton momentum from the QE interaction is usually below the Cherenkov threshold, the signal has only a single electro-magnetic shower ring (1Re).

The standard SK atmospheric neutrino analysis criteria are used to select 1Re events: single ring, electron like (showering), visible energy greater than 100 MeV, and no decay electrons. Reduction of number of events by the “standard” 1-ring e-like cut for charged and neutral current events are listed in Table 3. The excellent e/μ separation capability and $\mu \rightarrow e$ detecting capability are key features of the effective elimination of ν_μ charged current and all of the inelastic events which contain charged π . The remaining background events at this stage are predominantly from single π^0 production through neutral current interactions and from ν_e contamination in the beam. In order to reduce the background events which come from π^0 , further cuts are applied based on following information; (1) angle between ν beam direction and e-like ring, (2) invariant mass of two photons assuming that the event contains two rings which cannot be separated by “standard” algorithm, (3) difference between single and double ring likelihood, (4) energy fraction of lower energy ring, $\frac{E(\gamma_2)}{E(\gamma_1)+E(\gamma_2)}$, assuming the event contains two rings. Table 3 lists the number of events after this e/π^0 separation. Extra rejection of an order of magnitude (23/247.1) in the ν_μ neutral current background is achieved with the signal acceptance of 152.2/203.7=75%. Fig. 12 (left) shows the reconstructed neutrino energy distributions for 5 years. The oscillation parameters of $\Delta m^2 = 3 \times 10^{-3}$ eV 2 and $\sin^2 2\theta_{13} = 0.1$ are assumed. A clear appearance peak is seen at the oscillation maximum of $E_\nu \sim 0.75$ GeV. The right plot of Fig. 12 show 90% and 3 σ limits as a function of the years of operation with the systematic uncertainty of background subtraction to be 2%, 5% and 10%. The sensitivity of $\sin^2 2\theta_{13} = 0.006$ at 90% confidence level can be achieved in five years of operation. Fig. 13 shows 90% C.L. contours of sensitivity for 5 year exposure assuming 10% systematic uncertainty in background subtraction.

9 Summary

In the K2K experiment, both the number of observed neutrino events and the observed energy spectrum at SK are consistent with neutrino oscillation. It is concluded that the probability that our measurements are explained by statistical fluctuation without oscillation is less than

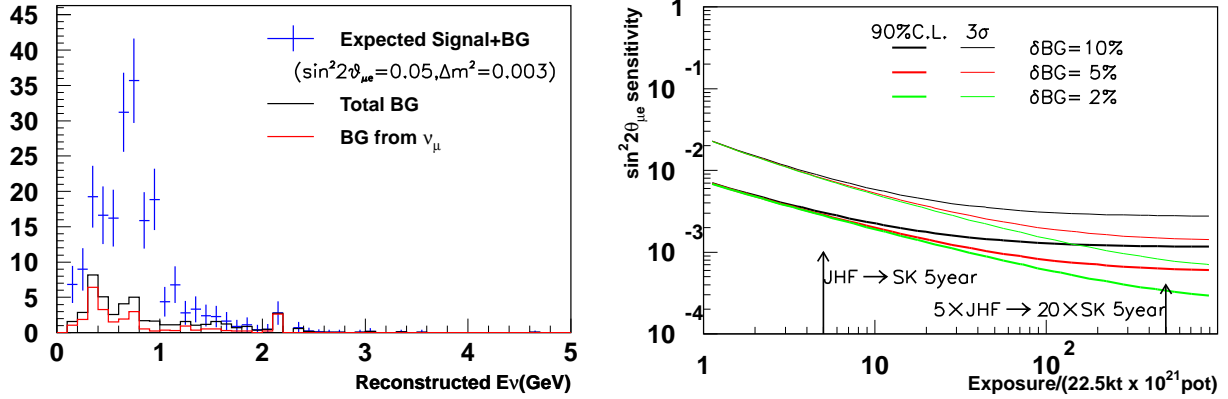


Figure 12: (Left) Expected reconstructed neutrino energy distributions of expected signal+BG, total BG, and BG from ν_μ interactions for 5 years exposure of OA2°. (Right) Expected 90%CL sensitivity (thick lines) and 3σ discovery contours (thin lines) as the functions of exposure time of OA2°. In left figure, expected oscillation signals are calculated with the oscillation parameters of $\Delta m^2 = 3 \times 10^{-3}$ eV 2 and $\sin^2 2\theta_{\mu e}$ (a effective mixing angle = $\sin^2 \theta_{23} \cdot \sin^2 2\theta_{13}$) = 0.05. In the right figures, three different contours correspond to 10%, 5%, and 2% uncertainty in the background estimation.

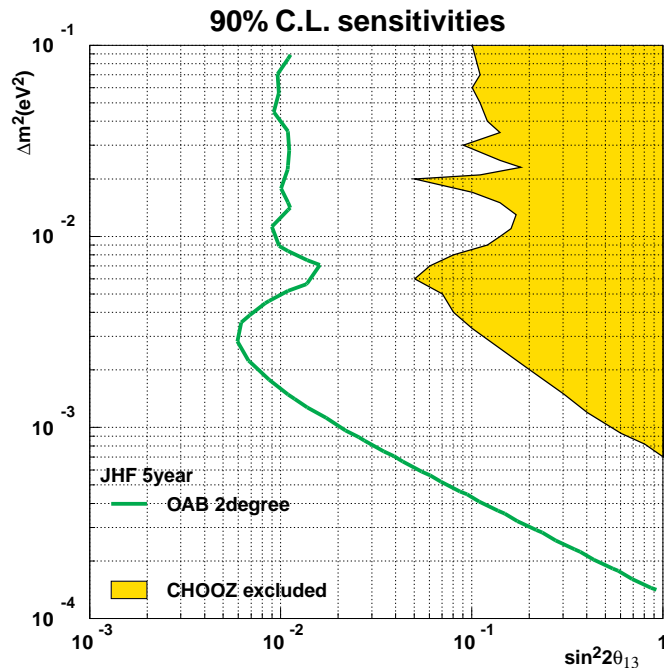


Figure 13: The 90% C.L. sensitivity contours in 5 years of operation with OA2°. The 90% C.L. excluded region of CHOOZ is plotted as a comparison. $\sin^2 \theta_{23}$ is assumed to be 0.5 and the possible contribution due to θ_{12} term is assumed to be small compared to the one due to θ_{13} term.

1%. The best-fit point in the oscillation parameter space is $(\sin^2 2\theta, \Delta m^2) = (1.0, 2.8 \text{ eV}^2)$ and the 90% C.L. region of Δm^2 at $\sin^2 2\theta = 1.0$ is $1.5\text{--}3.9 \times 10^{-3} \text{ eV}^2$, which agrees well with the atmospheric neutrino observations by Super-Kamiokande. After the accident of Super-Kamiokande in November 2001, the reconstruction work have been done by the beginning of December 2002, and K2K is now running, as K2K-II, to collect 2 times more data, and finally up to planned $\sim 10^{20}$ POT. As the upgrade of K2K near detectors, SciBar detector will fully installed in summer of 2003. The SciBar detector will enable us to study lower energy neutrino interactions and cross-section of neutrino interactions.

In order to confirm precisely the results of the first generation neutrino experiments and to explore the physics beyond the Standard Model, JHF to Kamioka neutrino experiment, JHF- ν experiment, is planned. With the use of high intensity neutrino beam, $\nu_\mu \rightarrow \nu_e$ oscillation will be explored down to $\sin^2 2\theta_{13} = 0.006$ at $\Delta m^2 \sim 3 \times 10^{-3} \text{ eV}^2$ with 90% C.L., which is 20 times higher sensitivity than CHOOZ experiment. The R&D has already started and the experiment is planned to start in 2007.

Acknowledgments

I gratefully acknowledge Prof. Y. Totsuka for his financial support to give me a precious opportunity to attend such a authoritative conference and give a talk there. I also thank the Japan Society for Promotion of Science (JSPS) for the support. The K2K experiment have been build and operated with the support from the Ministry of Education, Culture, Sports, Science and Technology, Government of Japan, by the U.S. Department of Energy, by the Korea Research Foundation, and by the Korea Science and Engineering Foundation.

References

1. Super-Kamiokande Collaboration, Y. Fukuda *et al.*, Phys. Rev. Lett. **81**, 1562 (1998).
2. K2K Collaboration, S.H. Ahn *et al.*, Phys. Lett. B **511**, 178 (2001).
3. K2K Collaboration, A. Suzuki *et al.*, Nucl. Instrum. Meth. A **453**, 165 (2000).
4. K2K MRD Group, T. Ishii *et al.*, Nucl. Instrum. Meth. A **482**, 244 (2002).
5. You can find descriptions on K2K experiment in some conference proceedings, for example, A.K. Ichikawa for the K2K collaboration, in the proc. of the XXXVIIth Rencontres de Moriond on Electroweak Interactions and Unified Theories, Les Arcs, France, 9–16 March 2002, e-print: hep-ex/0206037.
6. K2K Collaboration, M.H. Ahn *et al.*, Phys. Rev. Lett. **90**, 041801 (2003).
7. Y. Yamanoi *et al.*, “Large Horn Magnet at the KEK Neutrino Beam Line – part2”, IEEE Trans. on Applied Superconductivity **10**, 252 (2000).
8. T. Maruyama, Ph.D. thesis, Tohoku University, 2000.
9. Super-Kamiokande Collaboration, Y. Fukuda *et al.*, Phys. Lett. B **433**, 9 (1998).
10. B.J. Kim *et al.*, Nucl. Instrum. Meth. A **497**, 450 (2003).
11. V. Bernard, L. Elouadrhiri, and U.G. Meissner, J. Phys. G **G28**, R1 (2002).
12. D. Rein and L.M. Sehgal, Nucl. Phys. **B223**, 29 (1983).
13. J. Marteau *et al.*, Nucl. Instrum. Meth. A **451**, 76 (2000).
14. M. Gluck, E. Reya, and A. Vogt, Z. Phys. C **67**, 433 (1995).
15. A. Bodek and U.-K. Yang, Nucl. Phys. **B112**, 70 (2002).
16. Y. Itow *et al.*, Letter of Intents for JHF- ν experiment (2001), e-print: hep-ex/0106019.
See also JHF- ν web site: <http://neutrino.kek.jp/jhfnu/>
17. For example, Y. Yamanoi *et al.*, KEK Preprint 9-225, November 1997.
18. D. Beavis, A. Carroll, I. Chiang *et al.*, Proposal of BNL AGS E-889 (1995).